Full-scale experiments on the reduction of propeller-induced aircraft interior noise with active trim panels

M. Misol[a,*]

[a] *German Aerospace Center, Institute of Composite Structures and Adaptive Systems Braunschweig, Germany*

Abstract

Results are presented of full-scale experiments on the active reduction of rotor-induced passenger cabin noise in a Dornier Do728 aircraft. Two active sidewall panels (smart linings) are used to reduce the sound pressure in a control region in front of the linings. The fuselage pressure distribution associated with the first five harmonics of a generic counter-rotating open rotor (CROR) engine is emulated with a loudspeaker array. Each smart lining is equipped with two inertial force actuators. It uses up to eight error microphones and implements an adaptive feedforward controller. The two smart linings are driven in parallel. A maximum SPL reduction of 11.3 dB is achieved in the controlled area. The mean SPL reduction over 18 microphones is 6.8 dB. At the most critical second frequency, a mean SPL reduction of 9.3 dB is achieved by the two smart linings working in parallel. It is observed that the SPLs near the lining (at the window seat positions) are significantly higher than the SPLs near the aisle. This leads to the conclusion that the major part of the sound energy is transmitted through the linings, which is seen as an argument for the suitability of the smart lining concept.

Keywords: aircraft, rotor noise, propeller noise, interior noise, active control, lining

1. Introduction

The active control of rotor noise in aircraft is an ongoing research topic for more then thirty years. Some approaches have been successfully implemented in aircraft (e.g. Saab 2000 or Bombardier Dash 8 Q 400). Different strategies were pursued to reduce the disturbing noise in the aircraft passenger cabin. One approach uses loudspeakers to reduce the interior sound pressure by altering the radiation impedance or by anti-sound (ANC). Early results of ANC in aircraft are documented by [1]. In this work, secondary loudspeakers are placed in the near field of the sound emitting surfaces of the fuselage. Assuming that the fuselage acts as a compact sound source, a small number of secondary loudspeakers is applied. Maximum SPL reductions of 7–15 dB are measured in approx. a quarter of a wavelength (less than 1 m) around the microphones. It is concluded, that the complexity and distributed nature of the sound radiation of the fuselage requires more secondary sources. Early flight test results of ANC are reported in [2] and [3]. Both groups use the same BAe 748 twin turbo-prop aircraft but with different ANC systems. [2] use 24 loudspeakers and 72 microphones to realize SPL reductions of 8–13 dB at three frequencies. In [3], 16 loudspeakers and 32 microphones are used to achieve SPL reductions of 3.7–14 dB at two frequencies. More details on the flight tests can be found in [4]. Results on ANC in a Saab 2000 aircraft are reported by [5]. The active control system uses 36 loudspeakers and 72 error microphones. The measured SPL reductions are 8–14 dB at the blade-passing frequency (BPF) and approx. 8 dB summed over the first three frequencies.

An alternative approach to ANC is the active control of the fuselage vibration by means of shakers or piezoelectric patch actuators. Depending on the error sensing scheme, this technique is either called

*Corresponding author
Email address: malte.misol@dlr.de (M. Misol)

active vibration control (AVC), active noise vibration control (ANVC) or active structural acoustic control (ASAC). Early results on ANVC in aircraft are documented by [6]. In this work, a model aircraft fuselage (downscaled unstiffened aluminum cylinder) is mounted in an anechoic chamber and excited by a monopole sound source. A mini-shaker is used as control actuator of the system. Strong reductions of interior SPL are reported with a single properly tuned actuator. First results of AVC experiments in a real aircraft are reported by [7]. The test setup is a 50 ft aft-section of a McDonnell Douglas DC-9 series 10 mounted in an anechoic room. The fuselage is excited at the pylons by one or two primary shakers. The secondary shakers, used for the active control, are placed in the interior side of the fuselage directly opposite to the primary shakers. By using up to four microphones as error sensors, the acoustic potential energy is reduced up to 13 dB at some frequencies. Only 5 dB reduction is achieved with one accelerometer as error sensor. Unlike other experiments, this work focuses on the structure-borne sound transmission path. Experiments on AVC in a deHavilland Dash-8 series 100/200 aircraft on ground are documented in [8]. The fuselage is excited by means of four loudspeakers positioned in the port rotor plane. A sound field synthesis method is applied to synthesize the pressure distribution on the fuselage. Actuator positions are derived by evaluating the operational deflection shapes of the frames at the BPF. Three frames are equipped with a large number of small interconnected piezoelectric patch transducers. The weighted average of the signals of four accelerometers per frame serves as the error signal of the feedback controller. Each frame is controlled by an independent single input single output (SISO) feedback loop. The maximum SPL reduction achieved by the AVC system is 8.4 dB evaluated at six microphones located at the seat positions. Flight tests of ASAC in a Raytheon 1900D aircraft are reported by [9]. The ASAC system uses 21 inertial actuators and 32 microphones. The actuators are mounted on the fuselage frames and the microphones are distributed in the passenger cabin. Control results with only one frequency (BPF) show a mean SPL reduction of 15 dB. In the multi-frequency case with three harmonics the mean SPL reduction drops to 10 dB. It is mentioned that the ASAC system is very energy efficient with a maximum power of 7 W per actuator. More recent research results are reported by [10] and [11]. In [10] an AVC system is designed for a stiffened carbon-fibre reinforced plastic (CFRP) panel excited by a synthesized CROR excitation. [10] use narrow band active feedback control (H_∞) instead of active feedforward control. This method requires no reference signals, but more attention is required in the design of the controller to guarantee robustness and stability. The AVC system achieves a vibration reduction up to 9.7 dB at the error sensors and a reduction of sound power up to 7.9 dB at one frequency. In [11] an optimized AVC feedforward control system is implemented on a fuselage partition of a Dornier Do728 aircraft. The experiments are performed on ground with a synthesized CROR pressure excitation. The active system uses 12 actuators and either 12 or 24 accelerometers as error sensors. A maximum sound power reduction of 3.4 dB was achieved on an average for the first five CROR frequencies.

A related structure-based approach for active interior noise reduction uses active trim panels (linings) instead of actuated fuselage structures. This method, which is also the focal point of this paper, has gained less attention by researchers compared to the other approaches. One reason might be the unsatisfactory performance of such systems reported by [12] and by [13]. In the experimental work of [12], the active linings are coupled to a stiffened fuselage barrel (3.66 m long with a diameter of 1.68 m) made of filament-wound graphite-epoxy composite, stiffened with frames and stringers and equipped with a plywood floor. The linings are generic sandwich structures extending from floor to floor. A loudspeaker is used for the excitation of the fuselage barrel, which is sealed with end caps to prevent flanking transmission. The whole setup is located in an anechoic chamber. Piezoelectric patch actuators are applied to the outer surface of the linings. A global SPL reduction of up to 5 dB is achieved by the active system, which is considered unsatisfactory, especially in view of the promising results documented by [6]. The limited performance of the active linings is explained (at least in parts) by the different coupling of primary excitation and active linings into the cavity modes. A similar behavior, although expected, was not observed in the experiments of [6]. In [13], full-scale experiments in a McDonnell Douglas DC-9 aircraft (on ground) are described. The active control system uses 16 piezoelectric patch actuators on the linings (aft section) and 32 microphones placed at the headrests and in the aisle. The measured noise reduction was basically limited to one frequency (out of eight), which is much less compared to loudspeaker-based systems (ANC) and systems with actuators on the fuselage that were implemented on the same aircraft [13, Fig. 4]. In conclusion, the unsatisfactory

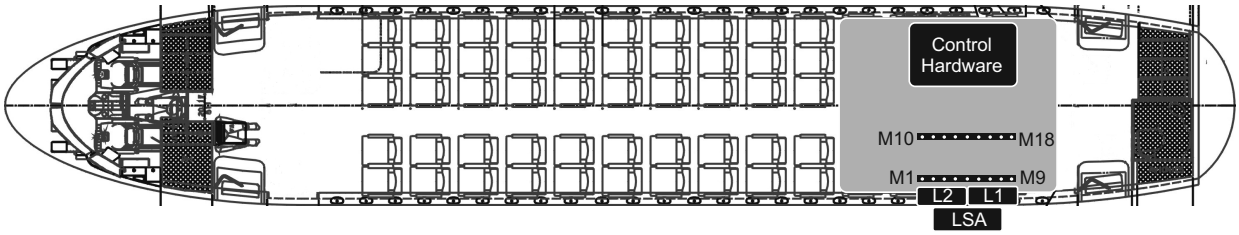

Figure 1: Overview of the experimental setup in the Dornier Do728 aircraft with loudspeaker array (LSA), the smart linings (L1 and L2) and the microphones M1 to M18.

performance of the active linings is explained by the unsuitable structural dynamics of the linings, the sub-optimal actuator positions and the flanking paths. As there is no further elaboration on these possible explanations, it remains unclear, which factors are most important for the limited performance and how these limitations could be overcome. Yet the results are very important, since a real aircraft is used for the experiments, which provides a test environment with realistic structural and acoustic damping. It is also the aim of the present contribution to assess the noise reduction performance of active linings in a realistic full-scale experiment [14]. In parallel to these full-scale investigations, experiments are done in a sound transmission loss facility with an original Airbus A350 lining [15, 16, 17]. Different aspects are investigated there, beginning with preliminary tests in [15] to demonstrate the capability of the approach followed by experiments aiming at the replacement of laboratory hardware by low cost components [16, 17] and the replacement of microphones by structural sensors and an acoustic filter [18, 19].

The use of active trim panels for interior noise reduction instead of active fuselage structures (with actuators on fuselage panels or frames) is considered beneficial for several reasons. Firstly, trim panels are not safety relevant aircraft components which makes it easier to implement in existing (retrofit) but also for new aircraft. Compared with ANC systems using loudspeakers in the cabin, the trim panel approach is more energy and mass efficient because the trim panel itself acts as a big loudspeaker membrane. Moreover, the loudspeaker capability of the active trim panels can also be used to replace the loudspeakers of the passenger announcement system. The major advantage and novelty of the so-called smart lining concept is that each active lining acts as an autonomous module having its own transducers and decentralized control unit. Since the smart linings are modular they can be placed at specific regions of the cabin; for example in the first or business class or in noisy areas of the aircraft. The loudspeaker capability of the smart linings could also be used for the reduction of internal noise sources by means of anti-sound or for noise masking (e. g. at positions near the galley or the lavatory). In this contribution it is shown, that two smart lining modules driven in parallel are able to reduce the noise in front of them without interference or destabilization. The use of inertial mass actuators instead of piezoelectric patch actuators is considered superior because of the lower voltages, the higher stroke even at low frequencies and the stronger linearity. A disadvantage of the smart lining approach compared to noise control applied to the fuselage is that the linings are a secondary noise source like other vibrating interior parts. Therefore, noise originating from the fuselage could transmit through other pathes like the ceiling panels or the floor. This is considered especially severe for distributed external noise sources like the turbulent boundary layer. For rotor engines the external noise is more localized and smart linings could be placed at seat rows near to the rotor plane. It is shown in this contribution that smart linings are especially useful for the reduction of multi-tonal rotor noise.

2. Experimental Setup

The DLR test aircraft Dornier Do728 is a ground test facility with a complete primary structure (no engines) and a fully equipped cabin. A cross-sectional view of the aircraft is shown in Fig. 1. Although most parts of the Do728 are original, it must be noted that this is not true for the linings. The Do728 cabin is equipped with linings made of glass-fiber reinforced plastic (GFRP) which are connected to the fuselage

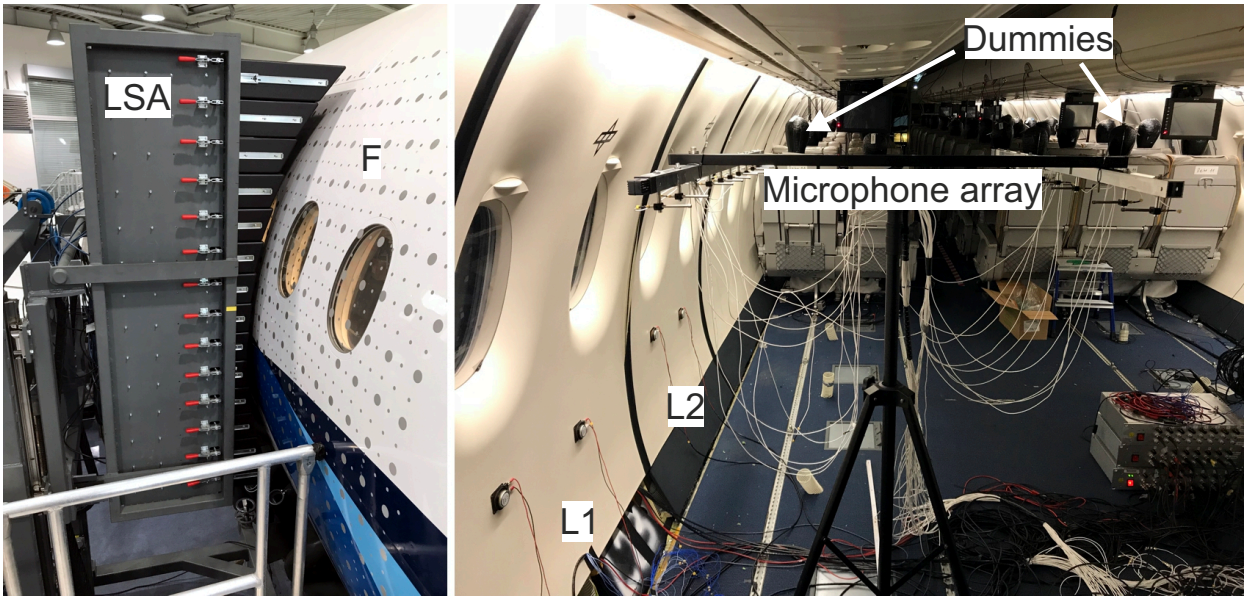

Figure 2: Experimental setup with loudspeaker array (LSA), aircraft fuselage (F) and smart linings (L1 and L2).

with simplified structural links and fixations. Despite these simplifications, the lining setup is useful and the derived results are considered meaningful for other aircraft as well. Experiments with a realistic aircraft double panel configuration with original parts support this assumption (see [15, 16, 17]). It is known from these experiments that the modal behavior of the fuselage-lining-system is very weakly pronounced. Therefore, a strong coupling of distinct structural modes with the cavity modes of the passenger cabin will not happen. In conclusion, the generic lining setup is well suited to reproduce the process of sound transmission into the passenger cabin. For reasons of convenience, the last four seat rows are removed (area indicated in light gray in Fig. 1). Fig. 2 shows a photograph of the experimental setup. Important components of this setup are the loudspeaker array (LSA), the aircraft fuselage (F) and the aircraft cabin with the two independent smart linings (L1 and L2). These parts will be described in more detail in the following subsections. A microphone array with 18 microphones of the type PCB T130D21 is placed in the cabin in front of the lining at a height of approx. 1.2 m.

Figure 3 shows a schematic of the experimental setup including the active components and signals of a smart lining. Inputs to the digital signal processing (DSP) are the microphone signals and the information about the excitation frequencies. The microphone signals are used as error signals for the adaptive feedforward control algorithm, while the frequencies of the LSA are used for the synthesis of the harmonic reference signals. For the experiments, it is assumed that the frequencies of the excitation do not vary over time. In real operating conditions, the reference signals containing the required frequencies are obtained from the rotary encoder signals capturing the rotational speeds of the engine shafts. In this case, the adaptive feedforward controller processes each reference signal and each frequency independently. The amplified (AMP) control signals are fed to the actuators of the smart lining.

2.1. Excitation

Rotor engines of aircraft induce high acoustic loads on the fuselage, which transmit into the cabin. The excitation frequencies depend on the rotational speed and the number of rotor blades. Simulation results of [20] derived for a generic counter-rotating open rotor (CROR) engine suggest that the strongest excitation occurs in the frequency range of 100–500 Hz. Therefore, the investigated active noise reduction system is designed for this frequency range, which contains the first five CROR frequencies (see first row of Table 1).

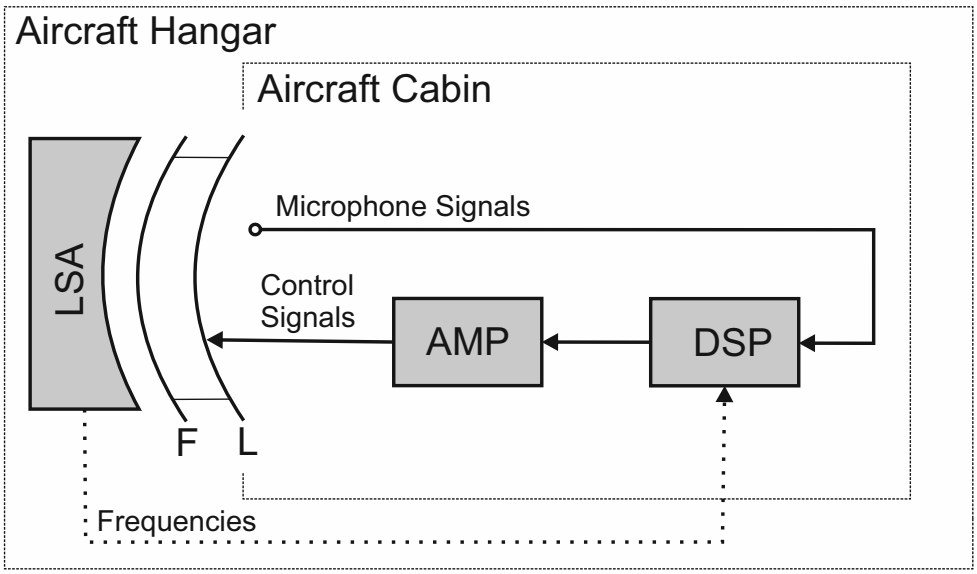

Figure 3: Schematic of the experimental setup showing the main signals and systems.

The synthesis of the calculated pressure distribution on the fuselage is done with a loudspeaker array (LSA) and a sound field reconstruction (SFR) method. As shown in Fig. 2, the LSA is placed in front of the fuselage at a distance of approx. 0.14 m. The LSA has 14 rows with eight loudspeakers each. In total, there are 112 loudspeakers, which can be individually controlled to facilitate the SFR. More information on the calculation and the synthesis of the CROR pressure field can be found in [20].

Table 1 lists the SPL measured outside and inside the aircraft at the CROR frequencies. The exterior SPL is measured with a microphone placed between LSA and fuselage in the center of the area covered by the LSA. The interior SPL is measured with a microphone placed in front of the lining at a distance of approx. 1 m. The values are intended to give a rough impression of the external and internal noise levels.

Table 1: Sound pressure levels outside and inside of the aircraft induced by the loudspeaker array.

F [Hz]	119.4	149.2	268.6	388.0	417.9
SPL out [dB]	109	110	108	93	106
SPL in [dB]	69	72	62	48	62

2.2. Aircraft

Preliminary tests of the smart lining were done in a sound transmission loss facility (see [15, 16, 17]). Tests in a fully equipped aircraft cabin provide the opportunity to achieve a more realistic acoustic environment compared to the acoustic laboratory (semi-anechoic room). Furthermore, two (or more) smart linings can be driven in parallel to assess robustness and cross-coupling between the individually controlled units. For the present investigation, the interior acoustics of the Do728 cabin is quantified by the reverberation time T_{60}. The measurement of T_{60} is done with a B&K Investigator 2260 with the reverberation time software BZ 7220, an OmniPower 4296 sound source and an amplifier 2716. The excitation noise is generated by the Investigator 2260 and fed to the amplifier. The whole process is controlled by the B&K measurement system. The outputs of this process are the reverberation times in third-octave bands as given in Table 2. It was observed in the experiments that at frequencies below 200 Hz, the value of T_{60} strongly depends on

the actual measurement position. This is attributed to the modal behavior of the cabin. Expected values of T_{60} of a single-aisle aircraft cabin (fully equipped but without passenger) lie in the range of 0.25–0.3 s. Values of T_{60} of an occupied cabin are not available, but it is assumed that the acoustic absorption of the human body will induce additional damping, which decreases T_{60}. Apparently, for frequencies above 160 Hz, the damping in the Do728 cabin is higher than the expected values. This is explained by the presence of dummies, which were installed in most parts of the cabin and might induce additional acoustic absorption. Although the dummies were designed for the thermal behavior of humans and hence will not correctly reflect the acoustic properties of a human body, they might increase the damping, which decreases T_{60}. Under this assumption, the obtained mean values of T_{60} are considered reasonable for the approximation of the acoustic environment of a fully occupied aircraft cabin.

Table 2: Measured reverberation times T_{60} in the aircraft cabin in third-octave bands.

F [Hz]	125	160	200	250	315	400	500
T_{60} [s]	0.37	0.41	0.14	0.19	0.18	0.21	0.22

2.3. Smart lining

Each smart lining is equipped with two inertial force actuators of the type Visaton EX 45 S. This type of actuator has a maximum power of 10 W (rms) and a mass of 0.06 kg. In order to ensure sufficient control authority, the structural vibration and interior SPL induced by the LSA are compared to the values generated by the actuators. It turned out that two actuators provide sufficient control authority. The positions of the actuators are not optimized. It is known from preliminary tests that the modal behavior of the coupled fuselage-lining-system is weakly pronounced and therefore, the actuator performance is not very sensitive regarding the location. However, it is known from measured FRF of 39 different actuator locations on an Airbus A350 lining that not all positions are equally suitable [19]. If the actuator locations are ranked according to the amplitudes of the acoustic FRF (actuator control voltage to error microphones), it turns out that the best actuator locations are on the skin field below the window units. In this analysis the amplitude difference between the best and the worst location on the lining surface (window regions excluded) were 7.8 dB. A more elaborate actuator placement based on genetic optimization is described in [15]. The microphones are mounted in two rows at a hight of approx. 1.2 m (see Fig. 4). This choice ensures an almost even spacing of microphones along the two linings and permits the measurement of SPL close to the lining and close to the aisle. The height of the microphones corresponds to the ear positions of the dummies (see Fig. 2). Two different error sensor configurations are considered. In configuration 1, each smart lining uses the same eight microphones M_1, M_4, M_7, M_9, M_{10}, M_{13}, M_{16} and M_{18} as error sensors. In configuration 2, L1 uses the microphones M_7, M_9, M_{16} and M_{18} as error sensors and L2 uses the microphones M_1, M_4, M_{10} and M_{13} as error sensors (see Fig. 4). The control algorithm is adopted from [21]. It is based on the complex filtered-x LMS algorithm and approximates the Newton algorithm [21, Eq. 5 and Eq. 8]. A block diagram of the adaptive feedforward control system is shown in Fig. 5. The harmonics Ω of the external pressure field are stored in the DSP. The reference signals X are filtered through the adaptive FIR filter W to produce the control signals U. Each actuator is controlled by one adaptive complex FIR filter weight for each harmonic. This permits a very efficient implementation even in the case of close frequencies (beating), which might arise if the rotors are not perfectly synchronized. Hence, each smart lining uses ten adaptive complex filter weights to control five harmonics with two actuators. The adaptive feedforward controllers of the smart linings are implemented on a dSPACE rapid control prototyping system.

The updates of the complex weights W_{rhl} of the FIR filter W are calculated according to Eq. (1). The current sampling instant at time t is indicated by n and the following sampling instant at time $t+T$ (with sample time T) is indicated by $n+1$.

$$W_{rhl}(n+1) = W_{rhl}(n) - 2\mu_{rhl} X^*_{rh}(n) \bar{\mathbf{G}}^H_{rhl} \mathbf{E}(n) \tag{1}$$

In this equation, W_{rhl} is the complex filter weight associated with actuator l and harmonic h of reference signal r. The complex numbers describing the frequency response function (FRF) of the secondary path G at the harmonics are stored in the matrix $\bar{\mathbf{G}}$. This method is very efficient compared to a state-space model (SSM) representation of G, which is sometimes used for time-domain broadband feedforward controllers. Furthermore, non-causal system configurations are described easily with the FRF and possible modelling errors of the identified SSM are avoided. This improves efficiency, robustness and disturbance rejection of the adaptive feedforward controller. The vector $\mathbf{E}$ contains the complex error signals. It is assumed that the reference signals X_{rh} are mutually uncorrelated. This assumption might be violated in steady flight conditions when the rotors are synchronized, but it is shown by [21] that in this case the redundant information will not lead to a reduced performance of a twin-reference controller compared to a single-reference controller.

The convergence factor μ_{rhl} comes from an approximation of the convergence factor matrix of the Newton algorithm [21, Eq. 8]. It is calculated according to Eq. (2).

$$\mu_{rhl} = \frac{\mu_0}{\rho_{rh} \sum_{m=1}^{M} \left|\bar{G}_{rhml}\right|^2} \tag{2}$$

The choice of this convergence factor is considered a good compromise between the robustness of the least mean squares (LMS) algorithm and the speed of the Newton algorithm. The convergence factor scaler μ_0 must be chosen carefully. Stability of the algorithm can be expected for positive values μ_0 smaller then one (though not guaranteed) [21]. In fact only substantially smaller values $\mu_0 \approx 0.001$ provided convergence. One reason could be the strong coupling of the actuators to the sensors and the corresponding weak approximation of the convergence factor matrix by a diagonal matrix. In further studies, Eq. (2) will be used to investigate this hypothesis and as a result possibly increasing the performance. The power of the reference signal rh is denoted by ρ_{rh}. It is set to unity in accordance to the unit amplitudes of the harmonic reference signals. Hence, the denominator of Eq. (2) equals the total power of the reference signal filtered through the secondary paths of actuator l to all M error sensors. The error sensor signals, which are sampled continuously by the DSP, are transformed into complex numbers without using the fast fourier transform (FFT). The implemented method is shown in the subsystem $t \rightarrow F$ of Fig. 6 at the example of a single-reference single-frequency single input multiple output (SIMO) system. After the analog-to-digital conversion (not shown), the time-domain error signals $\mathbf{e}$ are filtered by a band-pass filter B_{11} with corner frequencies of $\pm 10\%$ of the harmonic frequency f_{11}. In order to correctly filter out close tones it could be necessary to decrease the width of the passband. An approximation of the quadrature component is obtained from a discrete time delay z^{-k} with $k = round\,(0.25/(f_{11}T))$. Since the complex error signals are calculated without the use of the FFT, the processing delay is small and the algorithm is able to track fast changes in the reference signals.

3. Results

A microphone array is used for error sensing and control performance evaluation. As described in the preceding subsection, two different error sensor configurations are applied and not all microphones are used as error sensors for the adaptive control. Fig. 7 shows the mean SPL spectra of all microphones in the uncontrolled as well as in the controlled case in configuration 1. The mean SPL spectra are calculated from the average power spectral density of all microphones in the uncontrolled and in the controlled case. A frequency resolution of 1 Hz is taken for the frequency domain calculations. The peak average SPL reduction is achieved at 149.2 Hz with 9.3 dB. The reductions at 119.4 Hz and 268.6 Hz are 7.7 dB and 7.1 dB. At 388 Hz and 417.9 Hz, no reductions are achieved. The reduction is limited because the number of microphones is larger than the number of actuators (overdetermined system). This means that four actuators on two linings cannot provide enough degrees of freedom for a significant SPL reduction at the eight error microphone locations. Since the SPL reduction is evaluated for these eight error microphones plus additional ten microphones at uncontrolled locations, it is necessarily limited. Referring to [22, Fig. 1], the limit to noise reduction is determined by the control source arrangement. If a higher noise attenuation is

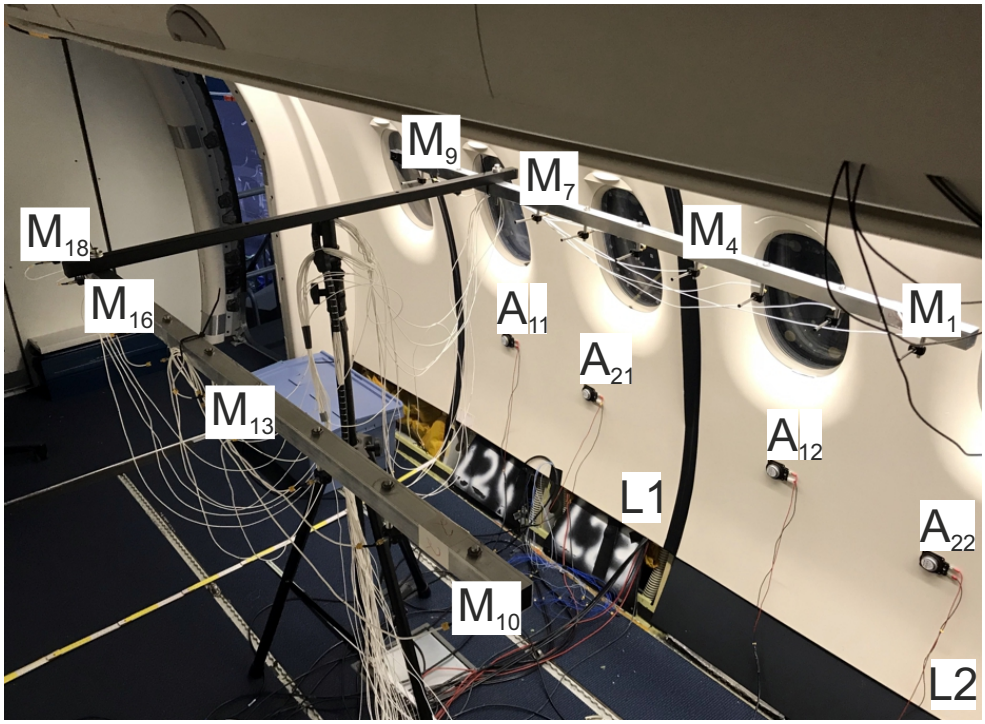

Figure 4: Smart linings (L1 and L2) with actuators (A) and sensors (M).

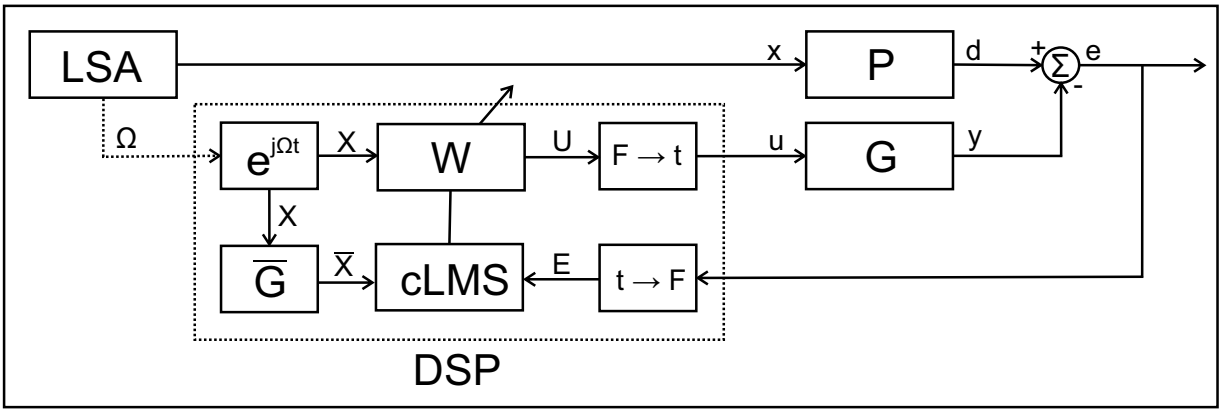

Figure 5: Block diagram of the adaptive feedforward control system.

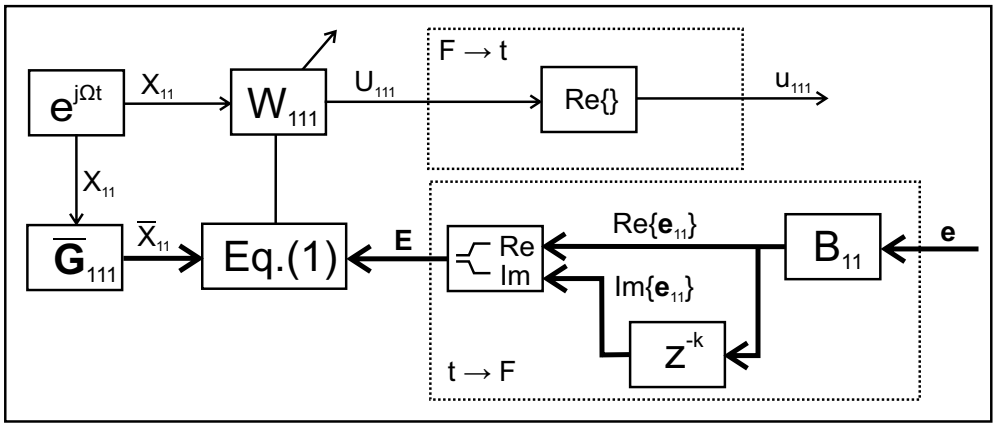

Figure 6: Block diagram of the signal processing with one reference signal ($r = 1$), one harmonic ($h = 1$) and one actuator ($l = 1$). Bold letters and thick lines indicate vectorial signals and systems.

required, the number of actuators must be increased. This reasoning can be substantiated by evaluating the theoretical maximum attenuation for a given configuration. From Fig. 5 it follows that a perfect cancellation of the disturbance pressures $\mathbf{d}$ requires the control signals $\mathbf{u}$ filtered through the secondary path $\mathbf{G}$ to be equal to $\mathbf{d}$. This requirement is reflected in Eq. (3), with $\mathbf{U}(k)$ and $\mathbf{D}(k)$ being the complex spectral values of the time domain signals $\mathbf{u}$ and $\mathbf{d}$ at CROR frequencies indexed by k.

$$\mathbf{D}(k) \stackrel{!}{=} \mathbf{G}(k)\mathbf{U}(k) \rightarrow \mathbf{U}_{opt}(k) = \left[\mathbf{G}(k)^H\mathbf{G}(k)\right]^{-1}\mathbf{G}(k)^H\mathbf{D}(k) \tag{3}$$

The theoretical maximum SPL reduction at frequency index k is obtained from Eq. (4). Since $\mathbf{G}$ is only known for the error microphones, the SPL reduction is not evaluated for the additional ten microphones at the uncontrolled locations. Therefore, the theoretical maximum SPL reductions listed in Table 4 are slightly higher than the mean SPL reduction obtained for 18 microphones.

$$\Delta L_{max}(k) = 10\log_{10}\frac{\mathbf{D}(k)^H\mathbf{D}(k)}{\left[\mathbf{D}(k) - \mathbf{G}(k)\mathbf{U}_{opt}(k)\right]^H\left[\mathbf{D}(k) - \mathbf{G}\mathbf{U}_{opt}(k)\right]}\,\mathrm{dB} \tag{4}$$

Table 4 shows the theoretical maximum SPL attenuation for the different configurations in Table 3.

Table 3: Different configurations of linings and error microphones.

Config.	Lining	Microphones
a	L1	M_7, M_9
b	L1	M_7, M_9, M_{16}, M_{18}
c	L1	M_1, M_4, M_7, M_9, M_{10}, M_{13}, M_{16}, M_{18}
d	L2	M_1, M_4
e	L2	M_1, M_4, M_{10}, M_{13}
f	L2	M_1, M_4, M_7, M_9, M_{10}, M_{13}, M_{16}, M_{18}
g	L1, L2	M_1, M_4, M_7, M_9
h	L1, L2	M_1, M_4, M_7, M_9, M_{10}, M_{13}, M_{16}, M_{18}

Recent research results of the author [18, 19] suggest the use of four actuators per lining instead of two. The increased actuator number provides more control authority for CROR engines producing external SPL up to 130 dB in front of the fuselage. A similar behavior to configuration 1 is observed in configuration 2,

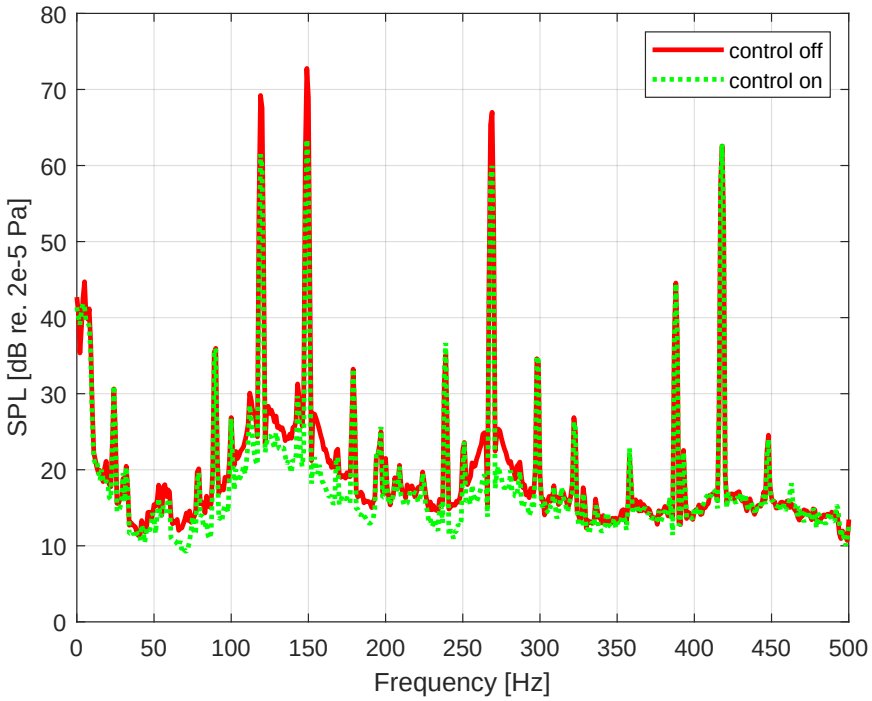

Figure 7: Mean SPL (average of M_1 to M_{18}) with inactive and active smart linings in configuration 1.

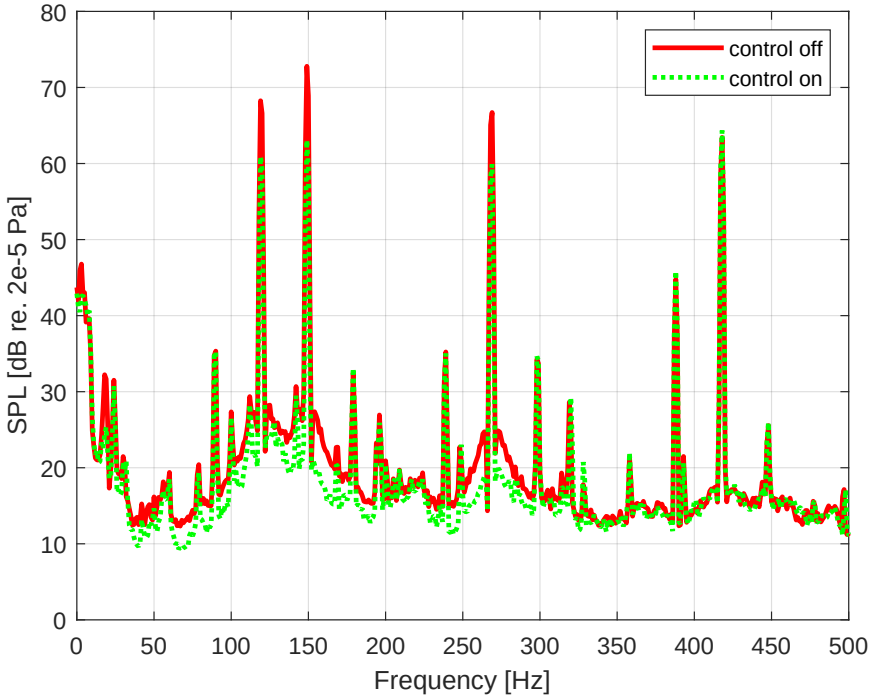

Figure 8: Mean SPL (average of M_1 to M_{18}) with inactive and active smart linings in configuration 2.

Table 4: Theoretical maximum SPL attenuation of the different configurations

Config.	$\Delta L_{max}(k_1)$	$\Delta L_{max}(k_2)$	$\Delta L_{max}(k_3)$	$\Delta L_{max}(k_4)$	$\Delta L_{max}(k_5)$
a	302.67	262.33	315.12	313.38	302.68
b	6.72	9.04	5.03	2.67	1.55
c	6.41	9.80	4.93	0.99	0.52
d	293.24	273.11	317.58	309.72	308.03
e	15.56	8.81	5.90	1.74	5.23
f	3.60	6.99	2.70	0.31	2.81
g	268.34	262.48	314.18	302.77	311.17
h	7.07	12.49	8.31	2.04	3.29

where each lining uses only four error sensors. Fig. 8 shows the mean SPL spectra of all microphones in the uncontrolled as well as in the controlled case in configuration 2. The mean SPL reductions are 7.4 dB at 119.4 Hz, 9.7 dB at 149.2 Hz and 6.8 dB at 268.6 Hz. At 388 Hz and 417.9 Hz, no reductions are achieved. The mean reduction of the rms values of the signals of all 18 microphones is 6.8 dB in configuration 1 and 6.3 dB in configuration 2.

The SPL distribution in front of the smart linings for both configurations is shown in Figs. 9 and 10. In the first row the uncontrolled SPL is contrasted to the controlled SPL with both smart linings active. In the uncontrolled case, the SPL near the linings (lower part) is approx. 10 dB greater than the SPL near the aisle (upper part). The decreasing SPL for an increasing distance between microphone and lining is seen as a consequence of the sound radiation of the lining and of the acoustic excitation of the fuselage partition the linings are mounted to. The first microphone row (M_1 to M_9) is approx. 0.4 m from the lining and the second microphone row (M_{10} to M_{18}) is approx. 1.2 m from the lining. Under ideal conditions, in an acoustic free field, the distance increase of a factor of three from the sound source would result in a SPL decrease of approx. 9.5 dB. Hence, the measured SPL decrease in the direction normal to the lining surface indicates that the main part of the acoustic energy is radiated by the linings. Since the remaining noise floor in the controlled case (Figs 9 and 10 top right) is on a similar level, the activated smart linings are not the dominant sound sources any more. Hence, the remaining SPL must be strongly influenced by other (uncontrolled) vibrating components or by flanking transmission. More measurements are necessary to corroborate this observation and to quantify the relative influence of the noise sources. The activated smart linings (SPL controlled L1&L2) achieve a relatively smooth SPL distribution in the monitored area with an average SPL of 69.8 dB for configuration 1 and 69.9 dB for configuration 2. The standard deviation of the SPL values drops from 3.6 dB in the uncontrolled case to 1.7 dB in configuration 1 and 2.1 dB in configuration 2. The second row of Figs. 9 and 10 shows the two cases when either one smart lining is switched off. In these cases, a smaller mean SPL reduction is observed with larger spatial variation of the SPL. According to Fig. 10, the inhomogeneous SPL reduction is particularly pronounced in configuration 2, which is a consequence of the error sensing scheme. It is concluded from these results, that a significant and uniform SPL reduction can be realized by the use of independent smart lining modules controlling the sound pressures in from of them. Since the linings are identified as the dominant factors for interior noise, the active system directly influences the sound transmission at the most relevant noise source. Under the assumption that the main sound energy is transmitted through the linings located in or near the rotor plane, a global SPL reduction in the passenger cabin seems possible by using a small number of smart linings. If other external or internal noise sources significantly contribute to the interior SPL, the assumption is violated and the achievable SPL reduction drops.

Table 5 lists the measured SPL of all microphones in the uncontrolled case (data from configuration 1) and the SPL reduction achieved by the two smart linings working in parallel either in configuration 1 or 2. As expected from Figs. 9 and 10, the maximum SPL reductions are achieved directly in front of the linings. This is a consequence of the higher SPL near the linings monitored by the microphones M_1 to M_9 (see Fig. 4

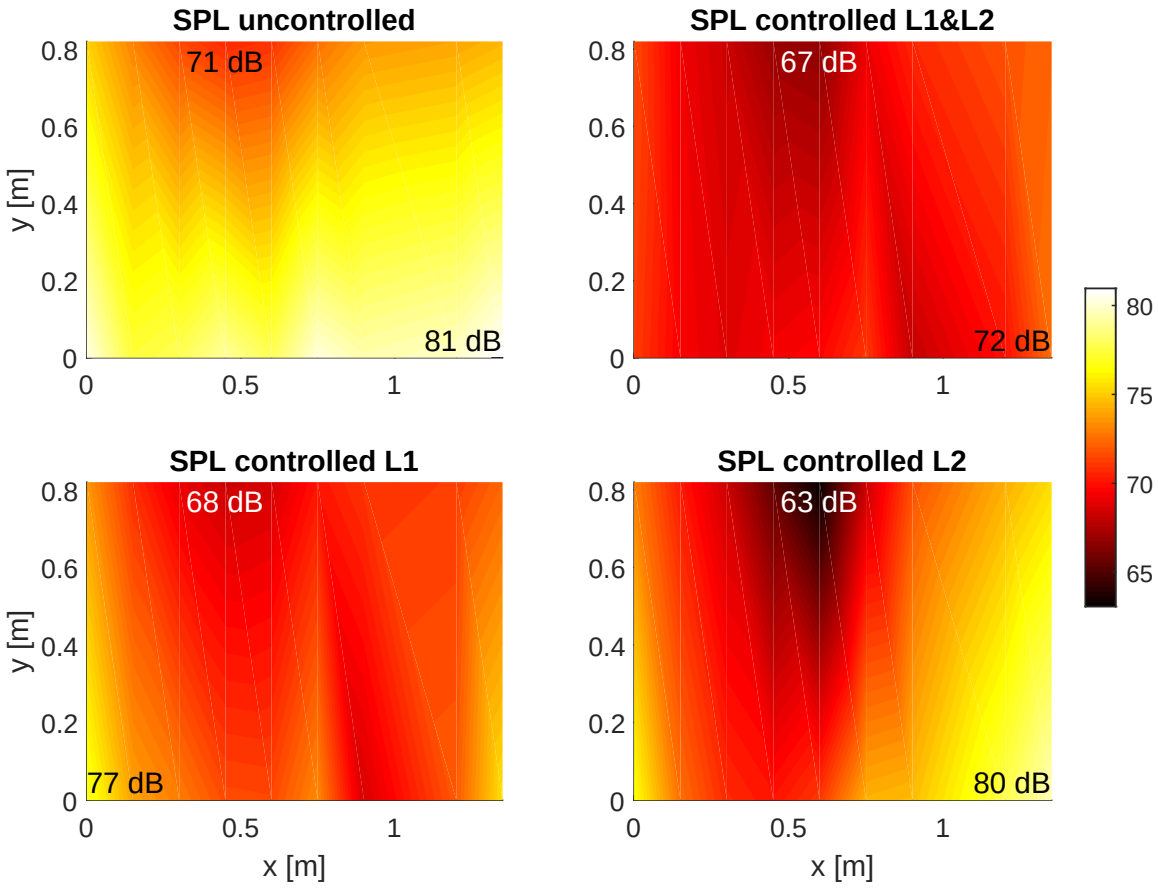

Figure 9: SPL distribution of configuration 1 in front of the smart linings in the uncontrolled case (top left), in the controlled case with both smart linings active (top right), in the controlled case with smart lining L1 active and L2 inactive (bottom left) and in the opposite case with smart lining L2 active and L1 inactive (bottom right). The x-axis is in parallel to the roll axis pointing to the aft and the y-axis is in parallel to the pitch axis pointing to the aisle. The (0,0) position coincides with the location of M_1.

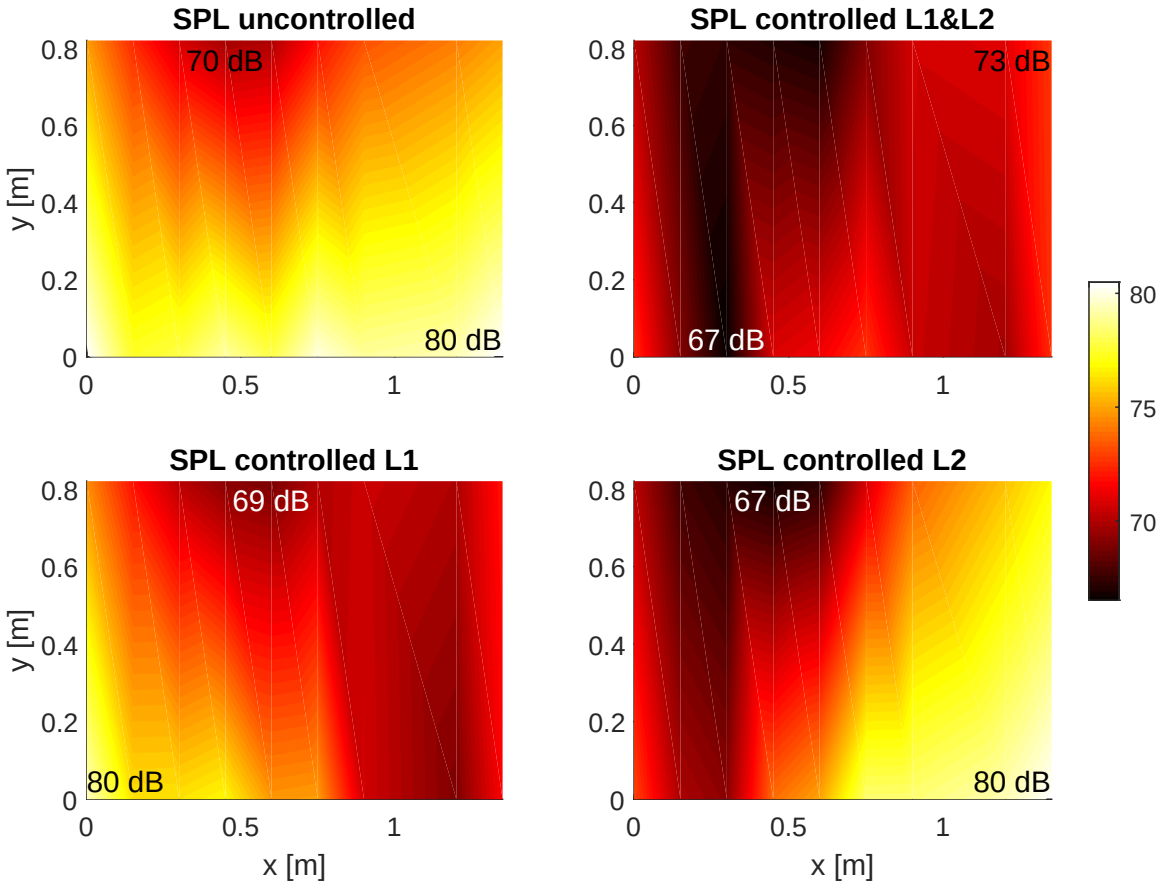

Figure 10: SPL distribution of configuration 2 in front of the smart linings in the uncontrolled case (top left), in the controlled case with both smart linings active (top right), in the controlled case with smart lining L1 active and L2 inactive (bottom left) and in the opposite case with smart lining L2 active and L1 inactive (bottom right). The axes definition is the same as in Fig. 9.

and Table 5).

Table 5: Sound pressure levels without control and reductions of the two error sensor configurations.

Microphone	M_1	M_2	M_3	M_4	M_5	M_6	M_7	M_8	M_9
SPL [dB]	80.4	77.4	77.9	79.1	77.9	80.2	79.4	79.9	81.0
SPL red. conf. 1 [dB]	9.3	7.9	9.1	9.7	8.2	9.2	11.3	9.9	8.5
SPL red. conf. 2 [dB]	8.0	8.3	11.3	8.2	6.5	7.3	8.5	9.7	7.9
Microphone	M_{10}	M_{11}	M_{12}	M_{13}	M_{14}	M_{15}	M_{16}	M_{17}	M_{18}
SPL [dB]	75.2	73.0	71.5	70.7	70.9	72.6	73.6	74.0	74.5
SPL red. conf. 1 [dB]	3.6	3.8	3.2	3.7	4.3	3.4	3.0	2.2	2.2
SPL red. conf. 2 [dB]	4.7	4.8	3.4	2.7	3.2	2.8	2.5	3.2	2.2

One possibility to overcome some of the limitations on SPL reduction is the application of a remote sensing scheme with virtual microphones as error sensors. The number and positions of these virtual microphones can be easily changed and adapted even in real-time control application (e. g. for head tracking applications [23]). An interesting application of virtual microphones for telephones is also provided in [24] where a zone of quiet is realized at at a virtual microphone location corresponding to the eardrum. Some results of the remote sensing scheme related to the active trim panels was recently published by the author [18].

4. Conclusion

In this work, a full-scale aircraft test setup is used to assess the noise reduction performance of so-called smart linings. A maximum SPL reduction of 11.3 dB is achieved in the controlled area. The mean SPL reduction over 18 microphones is 6.8 dB in configuration 1 (eight error sensors per lining) and 6.3 dB in configuration 2 (four error sensors per lining). At the most critical second frequency, a mean SPL reduction of 9.7 dB is achieved by the two smart linings working in parallel in configuration 2. The activated smart linings achieve a smooth and nearly uniform SPL distribution in the monitored area with an average SPL of 69.8 dB in configuration 1 and 69.9 dB in configuration 2. It is observed that the SPLs near the linings (at the window seat positions) are significantly higher than the SPLs near the aisle. This leads to the conclusion that the major part of the sound energy is transmitted through the linings, which is seen as an argument for the suitability of the smart lining concept. The experimental results suggest, that passive linings located in or close to the rotor plane should be upgraded to smart linings in order to achieve strong and global SPL reductions in the passenger cabin.

Current and future work is focused on an increase of the technology readiness level of the smart lining. Important steps towards this goal are the replacement of laboratory hardware by low-cost components (e. g. replacement of dSPACE with a microcontroller unit [16, 17]) and the optimization of the number and the locations of the actuators and sensors [19, 25]. To improve the modularity of the smart lining, it is desirable to replace the microphones by accelerometers mounted on the smart lining [18]. The remote sensing scheme with virtual microphones reduces the wiring effort on the one hand but increases the controller complexity on the other hand. As described in the preceding chapter, the use of virtual instead of physical error microphones provides more flexibility or even adaptivity with regard to the locations of the zones of quiet. Furthermore, experiments in the Do728 are planned to assess the performance and robustness of a larger amount of smart lining modules.

References

[1] J. M. Zalas, J. Tichy, Active attenuation of propeller blade passage noise, Tech. rep., NASA (1984).

[2] C. Dorling, G. Eatwell, S. Hutchins, C. Ross, S. Sutcliffe, A demonstration of active noise reduction in an aircraft cabin, Journal of Sound and Vibration 128 (2) (1989) 358–360.

[3] S. Elliott, P. A. Nelson, I. M. Stothers, C. C. Boucher, Preliminary results of in-flight experiments on the active control of propeller-induced cabin noise, Journal of Sound and Vibration 128 (2) (1989) 355–357.
[4] S. J. Elliott, P. A. Nelson, I. M. Stothers, C. C. Boucher, In-flight experiments on the active control of propeller-induced cabin noise, Journal of Sound and Vibration 140 (2) (1990) 219–238.
[5] U. Emborg, F. Samuelsson, J. Holmgren, S. Leth, Active and passive noise control in practice on the saab 2000 high speed turboprop, in: Proceedings of the 4th AIAA/CEAS Aeroacoustics Conference, 1998.
[6] C. R. Fuller, J. D. Jones, Experiments on reduction of propeller induced interior noise by active control of cylinder vibration, Journal of Sound and Vibration 112 (2) (1987) 389–395.
[7] M. A. Simpson, T. M. Luong, C. R. Fuller, J. D. Jones, Full-scale demonstration tests of cabin noise reduction using active vibration control, Journal of Aircraft 28 (3) (1991) 208–215.
[8] A. Grewal, D. G. Zimcik, L. Hurtubise, B. Leigh, Active cabin noise and vibration control for turboprop aircraft using multiple piezoelectric actuators, Journal of Intelligent Material Systems and Structures 11 (6) (2000) 438–447.
[9] D. Palumbo, R. Cabell, B. Sullivan, J. Cline, Flight test of active structural acoustic noise control system, Journal of Aircraft 38 (2) (2001) 277–284.
[10] S. Algermissen, M. Misol, T. Haase, O. Unruh, H. P. Monner, Active Structural Acoustic Control of Rotor Noise Transmission, in: Proceedings of the ECCOMAS Thematic Conference on Smart Structures and Materials (SMART2013), 2013.
URL https://elib.dlr.de/83693/
[11] T. Haase, O. Unruh, Active control of counter-rotating open rotor interior noise in a dornier 728 experimental aircraft: Optimised sensor placement, Acta acustica united with Acustica 102 (2016) 361–372.
[12] K. H. Lyle, R. J. Silcox, A study of active trim panels for interior noise reduction in an aircraft fuselage, in: SAE Technical Paper, SAE International, 1995.
[13] B. N. Tran, G. P. Mathur, Aircraft interior noise reduction tests using active trim panels, in: Proceedings of Noise-Con 96, 1996, pp. 395–400.
[14] M. Misol, Experiments on noise reduction in aircraft with active sidewall panels, in: 25th International Congress on Sound and Vibration, Silesian University of Technology Press, 2018, pp. 1–7.
URL https://elib.dlr.de/121168/
[15] M. Misol, T. Haase, S. Algermissen, V. Papantoni, H. P. Monner, Lärmreduktion in Flugzeugen mit aktiven Linings, in: Smarte Strukturen und Systeme – Tagungsband des 4SMARTS-Symposiums, 2017, pp. 329–339.
URL https://elib.dlr.de/112911/
[16] M. Misol, S. Algermissen, M. Rose, H. P. Monner, Aircraft lining panels with low-cost hardware for active noise reduction, in: Joint Conference ACOUSTICS 2018, 2018.
URL https://elib.dlr.de/122049/
[17] M. Misol, S. Algermissen, M. Rose, On the noise reduction of active sidewall aircraft panels using feedforward control with embedded systems, in: International Conference on Noise and Vibration Engineering 2018, Proceedings of ISMA, Katholieke Universiteit Leuven, 2018.
URL https://elib.dlr.de/123044/
[18] M. Misol, ACTIVE SIDEWALL PANELS WITH REMOTE MICROPHONE TECHNIQUE FOR AIRCRAFT INTERIOR NOISE REDUCTION, in: Proceedings of the 26th International Congress on Sound and Vibration, 2019.
[19] M. Misol, S. Algermissen, Remote Sensing for a Lining Integrated Active Structural Acoustic Control System, in: X. Martinez, H. Schippers (Eds.), European Conference on Multifunctional Structures (EMuS), International Centre for Numerical Methods in Engineering (CIMNE), 2019, pp. 24–29.
URL https://elib.dlr.de/128067/
[20] S. Algermissen, S. Meyer, C. Appel, H. P. Monner, Experimental synthesis of sound pressure fields for active structural acoustic control testing, Journal of Intelligent Material Systems and Structures 25 (7) (2014) 881–889.
[21] S. Johansson, P. Sjösten, S. Nordebo, I. Claesson, Comparison of multiple- and single-reference mimo active noise control approaches using data measured in a dornier 328 aircraft, International Journal of Acoustics and Vibrations 5 (2) (2000) 77–88.
[22] C. H. Hansen, X. Qiu, C. Petersen, C. Howard, S. Singh, ACTIVE NOISE AND VIBRATION CONTROL SYSTEM DESIGN CONSIDERATIONS, MECHANICS 26 (2) (2007) 37–46.
[23] S. J. Elliott, W. Jung, J. Cheer, Head tracking extends local active control of broadband sound to higher frequencies, Scientific Reports 8 (1) (2018) 5403.
URL https://doi.org/10.1038/s41598-018-23531-y
[24] M. Pawelczyk, Analog Active Control of Acoustic Noise at a Virtual Location, IEEE Transactions on Control Systems Technology 17 (2) (2009) 465–472. doi:10.1109/TCST.2008.2000988.
[25] S. Algermissen, M. Misol, A. Kokott, T. Haase, K. Gonet, V. Lungaho, Towards a Lining Integrated Active Structural Acoustic Control System, in: X. Martinez, H. Schippers (Eds.), European Conference on Multifunctional Structures (EMuS), 2019, pp. 30–37.
URL https://elib.dlr.de/127884/